ADVANCED FUNCTIONAL MATERIALS
www.afm-journal.de

Plasmon Mediated Near-Field Energy Transfer From Solid-State, Electrically Injected Excitons to Solution Phase Chromophores

*Jesse A. Wisch, Xiao Liu, Patrick J. Sarver, Cesar N. Prieto Kullmer, Agustin Millet, David W. C. MacMillan, and Barry P. Rand**

An organic diode is demonstrated that near-field energy transfers to molecules in solution via surface plasmon polaritons, in contrast to typical far-field excitation via absorption of traveling photons. Electrically generated excitons couple to surface plasmon modes in the cathode; the plasmons subsequently excite chromophore molecules on top of the cathode. External quantum efficiency and time resolved photoluminescence measurements are used to characterize the diode and the near-field energy transfer process. In addition, it is shown that excited chromophores can charge-transfer to quencher molecules, illustrating the potential of this device to be used for photochemical applications.

1. Introduction

Organic semiconductors (OSCs) have received considerable research interest in recent decades for applications including displays, lighting, and solar cells. While OSCs have relatively poor electronic properties (i.e., carrier mobility, morphological and molecular stability) when compared to inorganic semiconductors, their photophysical properties- including high luminescence quantum yields, high absorption coefficients, and synthetic tunability- give considerable merit to organic optoelectronic devices. The success of organic light-emitting diodes (OLEDs)[1–3] has shown that the merits of OSCs are sufficient for commercial viability. Furthermore, the photophysical properties of organic dyes and chromophores have unlocked many solution-phase applications, such as photoredox catalyzed organic synthesis,[4] visible-light catalyzed hydrogen evolution,[5] triplet fusion upconversion catalysis,[6] and fluorescent probe bioimaging.[7]

For solution-phase applications, organic chromophores are typically excited with far-field light sources such as lamps and lasers. This requires that a photon emitted by the light source is appropriately "guided" to the chromophore without parasitic absorption, reflection, or scattering. In addition, far-field photons from an excitation source can convolute signals emitted from a sample. In contrast to far-fields, where energy transfer processes are mediated by traveling photons, near-field energy transfer processes are mediated by localized virtual photons.[8] Near-field energy transfer to chromophores can have several advantages over far-field transfer. For example, a near-field is "invisible" in the absence of an absorptive medium, and thus cannot convolute signals emitted from a sample. In addition, the non-traveling virtual photons that mediate energy transfer do not require "guidance" as do far-field photons, because the near-field energy transfer process relies on an acceptor being located within the near-field.

However, in order to harvest the benefits of near-field energy transfer, a suitable medium to host near-fields is required. The near-field of surface plasmon polaritons (SPPs) can mediate energy transfer to chromophores; SPPs are quasiparticles that represent coupled photons and delocalized electrons, and can travel along metal/dielectric interfaces with a concomitant near-field decaying perpendicularly to the interface.[9] Previous work[10] has shown that donor chromophores can couple to SPP modes in a metallic thin film, and this generated SPP near-field can excite acceptor chromophores.

In this work, we demonstrate an organic optoelectronic diode that achieves near-field energy transfer to molecules in solution via SPPs. The schematic for the plasmon mediated energy transfer (PMET) diode is shown in **Figure 1**A. In contrast to the common transparent-substrate-emitting

J. A. Wisch, X. Liu, B. P. Rand
Department of Electrical and Computer Engineering
Princeton University
Princeton, NJ 08544, USA
E-mail: brand@princeton.edu
P. J. Sarver, C. N. Prieto Kullmer, A. Millet, D. W. C. MacMillan
Merck Center for Catalysis
Princeton University
Princeton, NJ 08544, USA
B. P. Rand
Andlinger Center for Energy and the Environment
Princeton University
Princeton, NJ 08544, USA
The ORCID identification number(s) for the author(s) of this article can be found under https://doi.org/10.1002/adfm.202214367.

DOI: 10.1002/adfm.202214367

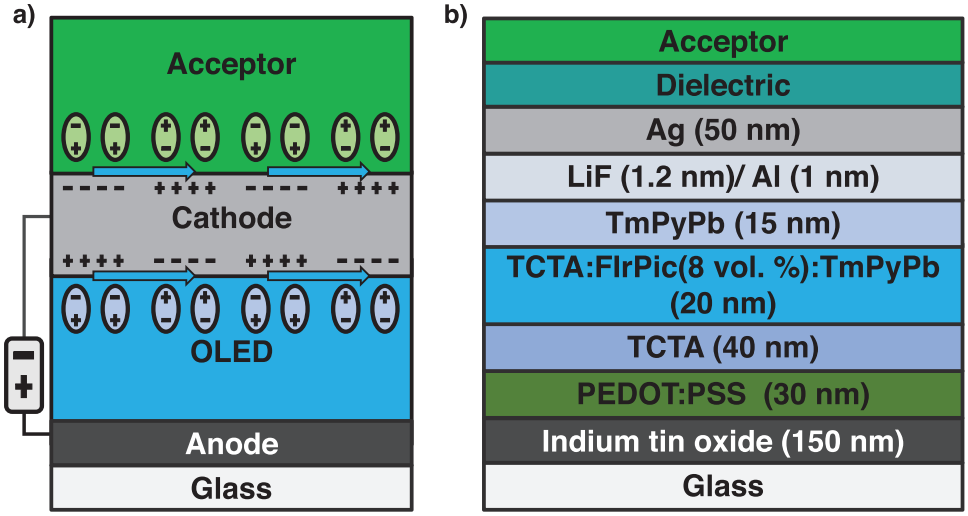

Figure 1. a) Conceptual schematic of the PMET diode. Donor excitons form in the EML and generate traveling SPPs in the silver cathode. The near-field of these SPPs excites acceptor molecules. b) Device stack of the PMET diode.

OLED that seeks to minimize coupling of emissive dipoles to SPP modes,[11] or scatters the non-emissive SPP modes into visible far-field photons,[12–13] the PMET diode seeks to maximize SPP coupling to excite acceptor molecules on top of the cathode. The PMET diode adopts the basic structure of an OLED, wherein a phosphor-doped emissive layer (EML) is sandwiched by electron/hole injection (EIL/HIL) and transport layers (ETL/HTL), shown in Figure 1B. Electrons and holes are injected from the cathode and anode, respectively, to form donor excitons in the EML. The silver cathode sustains traveling SPPs generated by donor excitons, and the evanescent near-field of these SPPs excites external acceptor molecules above the cathode. A thin-film high refractive index (n) dielectric layer above the cathode increases outcoupling to the acceptors. Using the PMET diode, we demonstrate excitation of solution-phase acceptors.

2. Results

To study the working mechanisms of the PMET diode, we measured both in-coupling of donor excitons to SPP modes and outcoupling of SPP modes to acceptors, and compared the results to electromagnetic simulations from code developed in Celebi et al.[15] To study in-coupling, we performed time-resolved photoluminescence (TRPL) measurements on the PMET diode while sweeping the distance between the EML donor excitons and the cathode by changing the thickness of the 1,3,5-tri(m-pyridin-3-ylphenyl)benzene (TmPyPb) ETL. Figure 1B shows the device stack for the PMET diode, based on the OLED reported by Chen et al.[14] with alterations made to improve outcoupling informed by the optical simulations. The donor molecule used in our structure is the common sky-blue OLED phosphor bis[2-(4,6-difluorophenylpyridinato-C^2,N](picolinato)iridium(III) (FIrPic). **Figure 2**A shows that the photoluminescence (PL) lifetime of the donor monotonically decreases from 1.17 to 0.60 μs as the ETL thickness is reduced from 70 to 15 nm, and matches well to the simulated trend. The decrease of PL lifetime is attributed to radiative decay rate enhancement from increased SPP in-coupling.[16] This result helps to inform device design to optimize the tradeoff between optoelectronic performance of the OLED structure and optical coupling to acceptors.

Outcoupling of SPPs-to-acceptor molecules was studied by measuring the top-emitting external quantum efficiency (TE-EQE) of the PMET diode with various thicknesses (2.5, 10, 20, 45 nm) of a low refractive index (n) dielectric (LiF) spacer between the cathode and an emissive acceptor layer. The SPP dispersion relation[17] reveals that lower refractive index dielectric claddings decrease the SPP optical density of states (DOS), thus LiF (n≈1.4) was chosen as a dielectric spacer to maximize the spacer-thickness dependence of SPP-to-acceptor coupling. This allows us to utilize relatively thin LiF spacer layers and minimize optical interference effects. A thin-film of the dye 4-(dicyanomethylene)-2-methyl-6-(4-dimethylaminostyryl)-4*H*-pyran (DCM) doped (20 vol. %) into a tris(8-hydroxyquinoline)aluminum(III) (Alq_3) host was used as the emissive acceptor layer, owing to its broad and intense absorptivity (≈1.36×10^5 M^{-1} cm^{-1}) that overlaps well with the donor emission (**Figure 3**A). We include a 10 nm neat Alq_3 layer separating the cathode from LiF to improve wetting. Identical devices without DCM dye were grown to control for far-field donor photons that escape through the silver cathode. The TE-EQE values from these control devices were subtracted from the DCM:Alq_3 device with identical LiF thickness, thereby isolating DCM emission. All EQE values were calculated assuming a Lambertian angular emission profile (simulations of angular emission profile shown in Figure S7, Supporting Information). As shown in Figure 2B, the average (over 1–100 mA cm^{-2} current density) TE-EQE drops from 1.42% to 0.36% as the LiF thickness increases from 2.5 to 45 nm. This nm-scale thickness dependence suggests that the DCM emission is near-field mediated. Furthermore, the experimental trend matches very well to the simulation.

We now demonstrate PMET diode operation with a solution-phase acceptor consisting of DCM dye (13 mM) dissolved in acetonitrile (MeCN) and calculate the quantum efficiency of

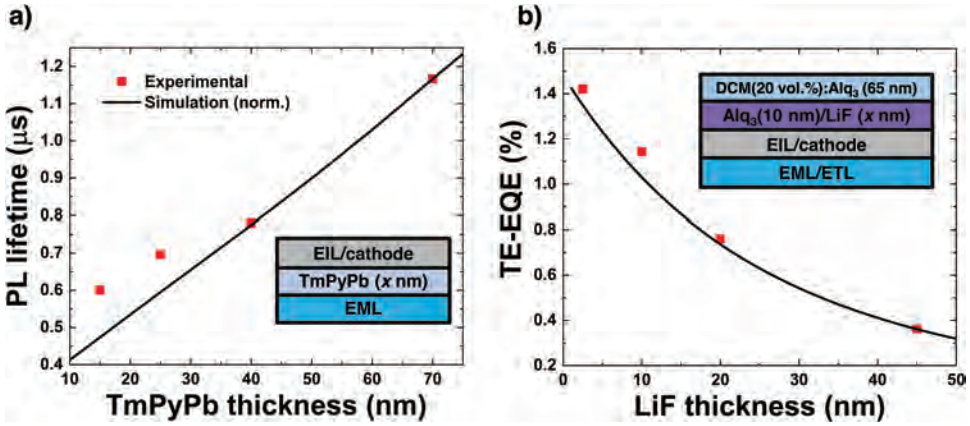

Figure 2. a) Excited state lifetimes determined by TRPL, with device structure for the experiment shown in the inset. As the ETL thickness increases from 15 to 70 nm, we see a monotonic increase in the PL lifetime (0.60, 0.70, 0.78, 1.17 μs) attributed to a lessening of the plasmonic radiative decay rate enhancement. Solid line shows simulated trend in lifetime, normalized to the max TmPyPb thickness. b) Average TE-EQE of the PMET diode with a solid-state acceptor separated from the cathode by various thickness of a LiF spacer. As the thickness of the spacer is swept from 2.5 to 45 nm, the TE-EQE drops, suggesting that emission originates from a near-field energy transfer process. Solid line shows simulated trend, normalized to the 45 nm LiF thickness.

the PMET (Φ_{PMET}) to DCM (that is, DCM molecules excited per electron injected). We found that choice of organic solvent and device materials were crucial in preventing dissolution and delamination of the PMET diode upon submersion. We chose MeCN as a solvent because it is nonaromatic and polar, and is also a commonly-used dye solvent. The structural contrast between MeCN and the nonpolar, aromatic small molecules used in the PMET structure discourages dissolution of the diode. To avoid delamination, poly(3,4-ethylenedioxythiophene) polystyrene sulfonate (PEDOT:PSS) was used as a wetting layer for the ITO anode. Solution-processed PEDOT:PSS can smoothen rough ITO surfaces,[18] encouraging more complete films. Furthermore, we capped the silver cathode with 6 nm of Al_2O_3 deposited via atomic layer deposition (ALD) to reduce penetration of MeCN into the device structure. To improve out-coupling to the acceptor, we evaporated 21 nm of TeO_2 (n≈2.2) on top of Al_2O_3, increasing the SPP optical DOS into MeCN.

To calculate Φ_{PMET}, we must consider that the solution-phase acceptor layer is limited to a much lower concentration of DCM than the solid-state layer due to the limited solubility

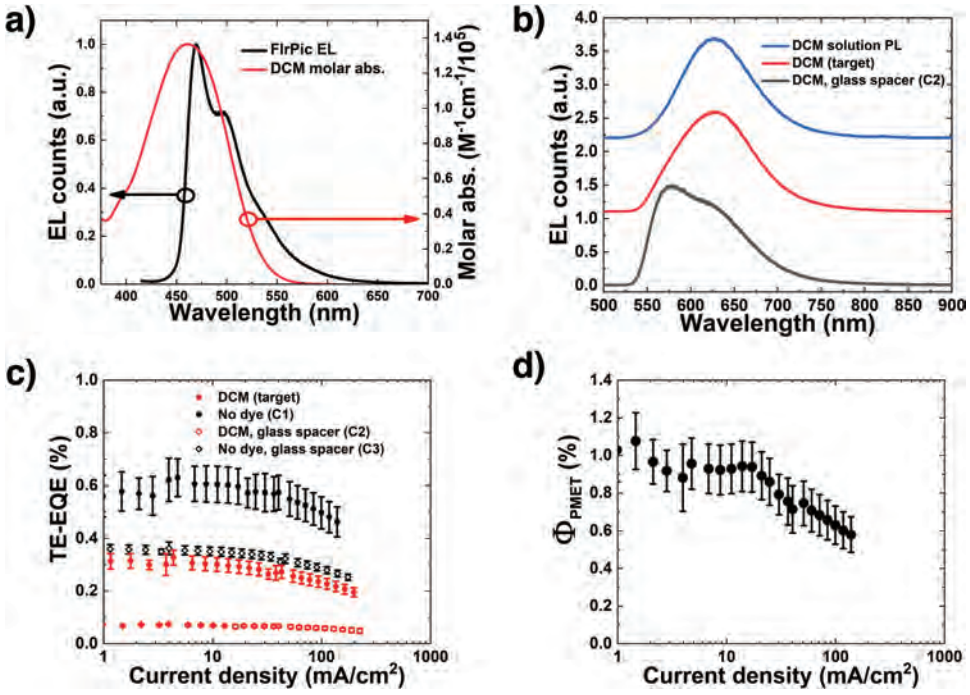

Figure 3. a) Molar absorptivity of DCM dye (red line) and EL of FIrPic (black line). b) Top-emitting EL spectra of DCM-acceptor PMET diodes, with and without a glass spacer. The PL of a 5 μM DCM solution in MeCN is included for reference. c) Top-emitting EQE versus current density of target device (red square) and three control devices d) Calculated Φ_{PMET} versus current density, from Equation 1.

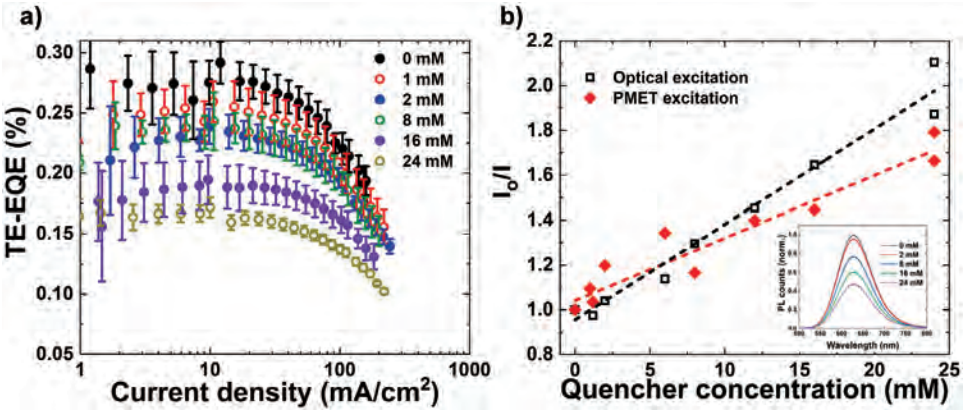

Figure 4. a) PMET diode TE-EQE versus current density with various concentrations of TMB added to dye solution. b) Stern-Volmer plots of DCM emission from PMET diode (red diamond) and conventional far-field optical excitation (black square). Inset shows PL spectra from photoexcited 13 mM DCM solution with various concentrations of TMB.

of DCM in MeCN (solution phase ≈8×10^{18} molecules cm^{-3}, solid-state ≈5×10^{20} molecules cm^{-3}). Since the strength of the SPP-coupling heavily depends on the absorption coefficient of the acceptor layer (see discussion for explanation), our solution phase device is thus limited to a weaker SPP-to-acceptor coupling than the solid-state device. As a result, the QE of DCM emission from PMET is comparable in magnitude to the TE-EQE of donor-emitted far-field photons that escape through the silver cathode.

We can control for the escaping far-field donor photons as well as sub-unity luminescence quantum yield of DCM by using a series of control devices in order to accurately calculate Φ_{PMET}. The first of these control devices (C_1) features neat MeCN as the acceptor layer, revealing the contribution of far-field donor photons to the target device TE-EQE. The neat MeCN preserves a similar optical environment (index of refraction) surrounding the OLED, but without any energy transfer to the solution. Furthermore, both the luminescence quantum yield and the fraction of DCM emission that escapes the device structure is unknown. Thus, we introduce a second control device (C_2) with a macroscopically-thick (150 μm) sheet of coverglass separating the thin-film device from the solution of DCM along with an identical device with neat MeCN (C_3). In both C_2 and C_3, there is no near-field energy transfer due to the many μm-thick coverglass separating the solution and the cathode. Since our 250 μm-thick solution of DCM absorbs ≈94% (absorbance calculated by convolving DCM absorptivity with FIrPic EL, Figure 3A) of the escaping far-field donor photons, the TE-EQE ratio of C_2 to C_3 is approximately equal to the probability that a DCM exciton will emit a detected photon. By measuring the TE-EQE of the target and the three control devices, we can calculate the Φ_{PMET}:

$$\Phi_{PMET} \cong EQE_{target}\left(\frac{EQE_{C3}}{EQE_{C2}}\right) - EQE_{C1} \quad (1)$$

In words, we are taking the number of DCM-emitted photons detected in the target device (EQE_{target}), dividing by the probability that a DCM excitation leads to a detected photon (EQE_{C2}/EQE_{C1}), and subtracting the QE contribution of far-field donor photons (EQE_{C1}). The TE-EQEs and calculated Φ_{PMET} are shown in Figure 3C,D, respectively. A peak Φ_{PMET} of 1.08% is achieved. It should be noted that this expression is a lower bound: roughly 6% of donor emission is not absorbed by DCM due to its broad red tail of emission, and thus the EQE ratio of C_3 to C_2 is artificially inflated. This spectral mismatch can be seen in Figure 3A, which includes donor electroluminescence (EL) and DCM absorption spectra.

Figure 3B shows the EL spectra of the C_2 and target devices, along with the photoluminescence (PL) spectrum of a 5 μM DCM in MeCN solution. We note that the target device EL closely resembles the DCM solution PL (628 nm) with a peak located at 626 nm, whereas C_2 has its primary peak at 578 nm and a secondary shoulder at ≈628 nm. We attribute this 578 nm peak in C_2 to the ≈6% of far-field donor photons that are not absorbed by the solution. These non-absorbed photons also contribute to the target device EL spectrum; however, because the target device features substantial emission from PMET, the contribution of the non-absorbed photons is minimal. This can be seen from the slight distortion of the EL Gaussian at ≈578 nm.

To demonstrate that the PMET-excited solution-phase acceptors can participate in a charge transfer reaction, we conducted Stern-Volmer luminescence quenching experiments. To do this, we measured the TE-EQE with various concentrations of a strongly electron-donating molecule, *N*,*N*,*N*',*N*'-tetramethylbenzidine (TMB) added to the dye solution. **Figure 4**A shows the TE-EQE measured from devices with 0, 1, 2, 8, 16, and 24 mM of TMB as a function of current density. As the concentration of TMB increases from 0 to 24 mM, the average TE-EQE from 1 to 100 mA cm^{-2} decreases from 0.26% to 0.16%. To extract the Stern-Volmer quenching rate k_q from these data, we divide the average TE-EQE with no quencher by that of each quenched device, and perform a linear fit to these points as shown in Figure 4B. This experiment was repeated with a separate batch of devices and solutions, and these additional points are also included in Figure 4B. The slope of this linear fit gives us k_q x τ_{PL}, where τ_{PL} is the zero-quencher PL lifetime of DCM in MeCN. We measured τ_{PL} (Figure S4B, Supporting Information) of a 13 mM DCM solution to be 1.6 ns. Assuming that τ_{PL} is unchanged between solution and the PMET diode surface, we get a k_q of $(17.2 \pm 1.6) \times 10^9$ M^{-1} s^{-1}. As a comparison, we measured the PL intensity of a photoexcited 13 mM DCM in MeCN solution as a function of TMB concentration, shown in the inset

of Figure 4B. This control gives a k_q of $(26.3 \pm 1.5) \times 10^9$ м$^{-1}$ s^{-1}. The decrease in the EL intensity with increasing TMB concentration implies that TMB decreases the luminescence quantum yield of DCM. Because TMB is an electron-rich molecule, it likely donates an electron to excited-state DCM, preventing photon emission. The k_q extracted from quenched PMET is a factor of 0.65 lower than the k_q from photoexcitation. This reduced k_q could be due to radiative decay rate enhancement of the DCM radiative emission rate from coupling to SPP modes, or due to increased collisional quenching with the PMET diode surface.

3. Discussion

We now discuss some of the design considerations for the PMET diode. The Φ_{PMET} defined in Equation 1 can be split into two components: the internal quantum efficiency (IQE) of the OLED (photons created per electron injected), and the outcoupling efficiency to the acceptor layer (acceptor molecules excited per emissive exciton formed). The IQE optimization of the PMET diode and of a display OLED are similar. For example, both devices benefit from including a triplet-harvesting emissive dopant[19] designing efficient electrodes,[20,21] or using high carrier mobility transport materials.[22] However, the PMET diode does not require a semitransparent anode, therefore a high-conductivity metal could be used in future devices to improve carrier injection.

To optimize outcoupling efficiency, we should avoid emitters with preferential in-plane dipole orientation,[23] since dipoles that are parallel to metal films couple much weaker to SPP modes than perpendicularly oriented dipoles. Also, as Figure 1A suggests, we should have a thin ETL. Furthermore, a high-index acceptor layer is desired because the SPP optical DOS increases with the refractive index of the dielectric cladding. However, the refractive index of most organic solvents is in the range of 1.3–1.5.[24] Depositing a thin solid-state high-index film on the cathode can increase the DOS in the low-index solvent. Here, we include a 21 nm TeO_2 ($n \approx 2.2$) layer.

Moreover, the strength of coupling from SPP modes to acceptor molecules depends heavily on the absorptivity of the acceptor layer, which is the product of the molar absorptivity and the concentration of the acceptor molecule. Intrinsically, SPPs are lossy and thus decay rapidly via thermalization; maximizing the concentration, and absorptivity of acceptor molecules increases the likelihood that an SPP will excite an acceptor molecule prior to thermalization. Laser dyes such as DCM, boron-dipyrromethene, fluorescein, and rhodamine are thus excellent photophysical candidates as PMET acceptors due to their high absorptivity[25] and solubility.

The thickness of the ITO, PEDOT:PSS, and TCTA layers were chosen with efficient hole injection in mind. Our optical simulations revealed that Φ_{PMET} did not depend heavily on the thicknesses of these layers, while the electronic performance depends on them heavily. The thickness of the emissive layer was chosen based on literature results.[14] The TmPyPb ETL thickness was chosen to be a thin 15 nm to increase plasmon in-coupling. A thin LiF layer was included to enhance electron injection, and a 1 nm Al layer was included to improve wetting of silver. The silver layer was chosen to be 50 nm, as our simulations suggested this thickness could allow for substantial plasmon-mediated energy transfer.

4. Conclusion

In this work, we have presented a device that transfers energy from electrically populated donor excitons to acceptor molecules via surface plasmon polaritons. We demonstrated the working mechanisms of the PMET diode using TRPL and EQE measurements, showed a 1.08% quantum efficiency for excitation of solution-phase acceptors, and showed that these near-field generated excitons can drive charge transfer reactions. For sensing applications, the PMET diode could excite fluorescent tags without introducing a parasitic excitation signal, which would be more difficult to execute with far-field excitation. Moreover, this device could enable electrically driven chemical reactions, a possibility we are currently investigating. This strategy would be well-suited to microscopically compact photochemical flow reactors, given the nanometer-scale excitation width. The local field enhancement from the SPPs could also be explored for triplet fusion upconversion, which often requires large fields to be enabled. Finally, this device could be explored for single-molecule spectroscopy as a means of providing low-background optical excitation.[26,27] Future work could explore optimization and applications of the PMET structure to target specific applications.

5. Experimental Section

Device Fabrication: Glass substrates with pre-patterned ITO with a sheet resistance of 15 Ω sq^{-1} were sonicated in soapy deionized water, deionized water, acetone, and isopropanol heated to 40 °C for 15 min each, followed by an O_2 plasma treatment for 10 min. The samples were subsequently spun-cast PEDOT:PSS (Clevios P VP AI 4083) on the ITO substrates at 4000 rpm with 4000 rpm s^{-1} acceleration and annealed in air at 140 °C for 10 min. The samples were then brought into a vacuum thermal evaporation (VTE) chamber (EvoVac, Angstrom Engineering, base pressure ~ 2×10^{-6} Torr) for thermal evaporation of 4,4′,4″-tris(carbazole-9-yl)triphenylamine (TCTA) (40 nm, deposition rate 1 Å s^{-1}), TCTA (0.5 Å s^{-1}): (FIrPic) (8 vol.%, 0.12 Å s^{-1}): TmPyPb (1 Å s^{-1}) (20 nm total), TmPyPb (15 nm, 1 Å s^{-1}), LiF (1.2 nm, 0.04 Å s^{-1}), Al (1 nm, 0.5 Å s^{-1}), and Ag (50 nm, 1 Å s^{-1}). For solution-phase acceptor experiments, the substrates were then placed into a Gemstar XT thermal atomic layer deposition system (Arradiance) with a chuck temperature of 80 °C to deposit Al_2O_3. Trimethylaluminum and water were alternatingly pulsed for 75 cycles, corresponding to an approximate Al_2O_3 thickness of 6 nm. The samples were then brought back into the VTE chamber to deposit 21 nm of TeO_2. For solid-state acceptor experiments, Alq_3 (10 nm, 1 Å s^{-1}), LiF (45 nm total, 0.2–1 Å s^{-1}), and DCM (20 vol.%, 0.2 Å s^{-1}): Alq_3 (1 Å s^{-1}) (65 nm total) were evaporated for target devices, or Alq_3 (65 nm, 1–2 Å s^{-1}) for control devices.

Optoelectronic Measurements: Saturated solutions of DCM (13 мм) and TMB (0–24 мм) were prepared in an N_2 glovebox using anhydrous MeCN. Approximately 100 µL of solution was placed onto the top of each device and sealed using a Thermo Scientific Gene Frame (Catalog Number: AB0578) and 150 µм-thick coverglass to prevent evaporation. The TE-EQE and current–voltage characteristics were measured using a customized setup consisting of a Keithley 2400 sourcemeter and a calibrated Si photodiode positioned perpendicular to the device (FDS-100-CAL, ThorLabs), measured with a picoammeter (4140B, Agilent). Steady-state

EL spectra were collected using SpectraPro HRS-300 spectrometer coupled with a PIX-400B CCD camera from Princeton Instruments. Transient photoluminescence decay curves were recorded using an FLS980 photoluminescence spectrometer (Edinburgh Instruments) with 375 nm excitation. Absorption spectra were recorded using a Cary 5000 UV—vis–NIR spectrometer (Agilent). Photoexcited Stern-Volmer measurements were conducted using a 450 nm laser diode excitation source and 1 cm path length quartz cuvettes. Device layer thicknesses were calibrated using variable angle spectroscopic ellipsometry (VASE) (Woollam M-2000 ellipsometer) of thin films on silicon.

Materials: Acetonitrile (anhydrous, 99.8%), DCM (Dye content 98%), TMB (≥ 95% HPLC), LiF (≥ 99.99% trace metals basis), and TeO_2 (≥ 99%) were purchased from Sigma–Aldrich. TCTA and FIrPic were purchased from Luminescence Technology Corporation. TmPyPb was purchased from Ossila Ltd. Alq_3 was purchased from Nichem. PEDOT:PSS (Clevios P VP AI 4083) was purchased from Heraeus and filtered with a 0.45 μm PTFE syringe-filter prior to spin-casting. All other materials were used without further purification.

Supporting Information

Supporting Information is available from the Wiley Online Library or from the author.

Acknowledgements

J.A.W. and X.L. contributed equally to this work. J.A.W., X.L., P.J.S., C.N.P.K., A.M., B.P.R., and D.W.C.M. acknowledge support from BioLEC, an Energy Frontier Research Center funded by the U.S. Department of Energy, Office of Science, Basic Energy Sciences under Award #DE-SC0019370. J.A.W., X.L., and B.P.R. acknowledge support from the Princeton Catalysis Initiative. P.J.S. thanks Bristol-Myers Squibb for a graduate fellowship. C.N.P.K. was supported by Princeton University, E. Taylor, and the Taylor family by an Edward C. Taylor fellowship.

Conflict of Interest

The authors declare no conflict of interest.

Data Availability Statement

The data that support the findings of this study are available from the corresponding author upon reasonable request.

Keywords

heterogeneous energy transfer, light matter interactions, organic light emitting devices, organic semiconductors, surface plasmon polaritons

Received: December 8, 2022
Revised: February 14, 2023
Published online:

[1] C. W. Tang, S. A. VanSlyke, *Appl. Phys. Lett.* **1987**, *51*, 913.
[2] M. A. Baldo, F. D. O'Brien, Y. You, A. Shoustikov, S. Sibley, M. E. Thompson, S. R. Forrest, *Nature* **1998**, *395*, 151.
[3] H. Uoyama, K. Goushi, K. Shizu, H. Nomura, C. Adachi, *Nature* **2012**, *492*, 234.
[4] C. K. Prier, D. A. Rankic, D. W. MacMillan, *Chem. Rev.* **2013**, *113*, 5322.
[5] J. Kosco, M. Bidwell, H. Cha, T. Martin, C. T. Howells, M. Sachs, D. H. Anjum, S. G. Lopez, L. Zou, A. Wadsworth, W. Zhang, L. Zhang, J. Tellam, R. Sougrat, F. Laquai, D. M. DeLongChamp, J. R. Durrant, I. McCulloch, *Nat. Mater.* **2020**, *19*, 559.
[6] L. M. Campos, T. Rovis, D. N. Congreve, E. M. Churchill, A. B. Pun, B. D. Ravetz, *Nature* **2019**, *565*, 343.
[7] T. Terai, T. Nagano, *Eur. J. Physiol.* **2013**, *465*, 347.
[8] T. Forster, *Ann. Phys.* **1948**, *6*, 55.
[9] W. L. Barnes, A. Dereux, T. W. Ebbesen, *Nature* **2003**, *424*, 824.
[10] P. Andrew, W. L. Barnes, *Science* **2004**, *306*, 1002.
[11] P. A. Hobson, J. A. Wasey, I. Sage, W. L. Barnes, *IEEE J. Sel. Top. Quantum Electron.* **2002**, *8*, 378.
[12] P. A. Hobson, S. Wedge, J. A. Wasey, I. Sage, W. L. Barnes, *Adv. Mater.* **2002**, *14*, 1393.
[13] M. A. Fusella, R. Saramak, R. Bushati, V. M. Menon, M. S. Weaver, N. J. Thompson, J. J. Brown, *Nature* **2020**, *585*, 379.
[14] Y. Chen, J. Chen, Y. Zhao, D. Ma, *Appl. Phys. Lett.* **2012**, *100*, 213301.
[15] K. Celebi, T. D. Heidel, M. A. Baldo, *Opt. Express* **2007**, *15*, 1762.
[16] W. L. Barnes, *J. Mod. Opt.* **1998**, *45*, 661.
[17] J. R. Sambles, G. W. Bradbery, F. Yang, *Contemp. Phys.* **1991**, *32*, 173.
[18] A. Kohler, B. Heinz, *Electronic Processes in Organic Semiconductors: An Introduction*, Wiley-VCH, Weinheim, **2015**.
[19] C. Adachi, M. A. Baldo, M. E. Thompson, S. R. Forrest, *J. Appl. Phys.* **2001**, *90*, 5048.
[20] Y. Zhou, C. Fuentes-Hernandez, J. Shim, J. Meyer, A. J. Giordano, H. Li, P. Winget, T. Papdopoulos, H. Cheun, J. Kim, M. Fenoll, A. Dindar, W. Haske, E. Najafabadi, T. M. Khan, H. Sojoudi, S. Barlow, S. Graham, J.-l. Bredas, S. R. Marder, A. Kahn, B. Kippelen, *Science* **2012**, *336*, 327.
[21] C. Wu, C. Wu, J. C. Sturm, A. Kahn, *Appl. Phys. Lett.* **1997**, *70*, 1348.
[22] S.-J. Su, T. Chiba, T. Takeda, J. Kido, *Adv. Mater.* **2008**, *20*, 2125.
[23] M. C. Gather, K. Leo, B. Lussem, M. Furno, C. Murawski, P. Liehm, *Appl. Phys. Lett.* **2012**, *101*, 253304.
[24] M. Konstantinos, M. Papamichael, S. C. Betsis, I. Stavrakas, G. Hloupis, D. Triantis, *Appl. Phys. B* **2014**, *116*, 617.
[25] K. H. Drexhage, in *Dye Lasers*, Springer, Berlin, **1990**.
[26] W. Moerner, Y. Shechtman, Q. Wang, *Faraday Discuss.* **2015**, *184*, 9.
[27] S.-C. Liu, B.-K. Xie, C.-B. Zhong, J. Wang, Y.-L. Ying, Y.-T. Long, *Rev. Sci. Instrum.* **2021**, *92*, 121301.